Monthly Notices
of the
ROYAL ASTRONOMICAL SOCIETY

MNRAS **527,** 7028–7035 (2024)
Advance Access publication 2023 November 27

https://doi.org/10.1093/mnras/stad3634

Kinematical coherence between satellite galaxies and host stellar discs for MaNGA and SAMI galaxies

Sen Wang,[1★] Dandan Xu,[1] Shengdong Lu[2] and Cheng Li[1]

[1]*Department of Astronomy, Tsinghua University, Beijing 100084, China*
[2]*Department of Physics, Institute for Computational Cosmology, Durham University, South Road, Durham DH1 3LE, UK*

Accepted 2023 November 20. Received 2023 November 20; in original form 2023 October 16

ABSTRACT

The effect of angular momentum on galaxy formation and evolution has been studied for several decades. Our recent two papers using IllustrisTNG-100 simulation have revealed the acquisition path of the angular momentum from large-scale environment (satellites within hundreds of kpc) through the circumgalactic medium (CGM) to the stellar discs, putting forward the co-rotation scenario across the three distance scales. In real observations, although the rotation signature for the CGM and environmental three-dimensional angular momentum are difficult to obtain, line-of-sight kinematics of group member galaxies and stellar disc kinematics of central galaxies are available utilizing existing group catalogue data and integral field unit (IFU) data. In this paper, we use (1) the group catalogue of SDSS DR7 and MaNGA IFU stellar kinematic maps and (2) the group catalogue of GAMA DR4 data and SAMI IFU stellar kinematic maps, to test if the prediction above can be seen in real data. We found the co-rotation pattern between stellar discs and satellites can be concluded with 99.7 per cent confidence level ($\sim 3\sigma$) when combining the two data sets. And the random tests show that the signal can be scarcely drawn from random distribution.

Key words: methods: data analysis – methods: observational – methods: statistical – galaxies: evolution – galaxies: formation – galaxies: kinematics and dynamics.

1 INTRODUCTION

As one of the most fundamental physical properties, angular momentum plays a key role for us to fully understand the formation and evolution of galaxies. A widely accepted theory explaining the origin of halo angular momentum is the tidal toque theory (Peebles 1969; Doroshkevich 1970; White 1984). The theory suggests that a dark matter halo gains angular momentum at the linear growth stage due to the misalignment between its inertia tensor and the tidal field tensor of the large-scale structure (LSS) around it, resulting in an alignment between the halo's angular momentum and its large-scale environment. When the evolution enters the non-linear regime, the LSS modulation becomes less efficient, gas cools and contracts within the dark matter halo. During this process, it spins up with angular momentum preserved, and becomes denser. Finally, star formation is triggered in the gaseous disc and a stellar disc eventually forms. Traditional models assume baryons acquire angular momentum from their dark matter haloes and define a specific angular momentum retention fraction, denoted by f_j. Usually f_j is close to 1 for disc galaxies (e.g. Mo, Mao & White 1998; Firmani & Avila-Reese 2000, 2009), which means baryons possess nearly the same amount of specific angular momentum as dark matter. In this sense, as a result, correlations in angular momenta must exist among the large-scale environment and the dark matter halo, the cold circumgalactic medium (CGM), and all the way down to the galaxy's stellar discs. During the non-linear structure growth, other processes such as gas shock-heating (White & Rees 1978; White & Frenk 1991) and galaxy mergers, also start to redistribute the angular momenta of the entire system, which tends to erase those correlations.

These correlations have been widely studied using cosmological simulations (e.g. Aragón-Calvo et al. 2007; Hahn et al. 2007; Libeskind et al. 2013a; Wang et al. 2018; López et al. 2021). In particular, Moon, An & Yoon (2021) studied the so-called spin-orbit alignment (SOA) of galaxy pairs in IllustrisTNG-100 simulation (Marinacci et al. 2018; Naiman et al. 2018; Nelson et al. 2018, 2019; Pillepich et al. 2018, 2019; Springel et al. 2018). They found significant alignment between the pair orbital angular momentum and the central star, gas, and DM spins, which only exists in central-satellite pairs, and the closer the stronger. Using cosmological N-body simulations, An et al. (2021) concluded that such SOA is possibly resulted from the local cosmic flow along the filament with a further growth due to neighbouring interactions. A recent paper series (Lu et al. 2022; Wang et al. 2022) using the Illustris TNG-100 simulation revealed the modulation of a galaxy's ambient angular momentum environment (i.e. the satellite galaxies) on the central star formation activeness, via the cold CGM gas. They demonstrated a significant signal of coherent rotation among the stellar disc, the cold CGM, and satellite galaxies (see fig. 9 of Lu et al. 2022). Similar coherent signals between spins of the DM halo and those from their neighbours were also confirmed by Kim, Smith & Shin (2022) using N-body simulations. Observationally, great efforts have also been

---

★ E-mail: wangsen19@mails.tsinghua.edu.cn made searching for correlated signals between galaxies/haloes and their LSS environment (e.g. Lee & Erdogdu 2007; Kraljic et al. 2021; Barsanti et al. 2022; Tudorache et al. 2022). In particular, kinematic coherence has been reported to exist with large significance using a sample of Calar Alto Legacy Integral Field Area (CALIFA) galaxies in their large-scale environment out to several Mpc (e.g. Lee et al. 2019a, b).

In this paper, we follow the predictions of Lu et al. (2022) and Wang et al. (2022) and investigate the correlations between a galaxy's stellar spin and the kinematics of the orbit motion of satellite galaxies in its neighbourhood. In particular, we search the signal using group catalogues of Sloan Digital Sky Survey (SDSS) and Galaxy And Mass Assembly (GAMA) surveys, and the corresponding integral field unit (IFU) observations therein, i.e. the Mapping Nearby Galaxies at Apache Point Observatory (MaNGA) and Sydney-Australian-Astronomical-Observatory Multi-object Integral-Field Spectrograph (SAMI), respectively. The paper will be organized as follows. In Section 2, we present the galaxy samples and the selection criteria. In Section 3, we describe the methods. In Section 4, the final results are shown. Finally, summaries and conclusions are presented in Section 5. The involved calculations in following sections adopt different cosmological parameters, with the tot matter density of $\Omega_{\rm m} = 0.238$, the cosmological constant of $\Omega_\Lambda = 0.762$, and the Hubble constant $h \equiv H_0/(100\,{\rm km s^{-1}\,Mpc^{-1}}) = 0.73$ for SDSS and MaNGA galaxies, and $\Omega_{\rm m} = 0.3$, $\Omega_\Lambda = 0.7$, $h = 0.7$ for the GAMA and SAMI galaxies.

2 GALAXY SAMPLES

2.1 The SDSS and MaNGA

The SDSS (York et al. 2000) is a large survey aiming at mapping a large field of sky by capturing images and taking spectra of distant objects. Until now, the SDSS has produced spectroscopic data for millions of galaxies and photometric data for even a lot more. A number of catalogues have been built up based on these data productions for different scientific goals. In this paper, we adopt the group catalogue constructed by Yang et al. (2007, hereafter YangDR7) using their own halo-based group finder. Applying this group finder to the New York University Value-Added Galaxy Catalog Data (Blanton et al. 2005) based on SDSS DR7 (Abazajian et al. 2009), they obtain 473 872 galaxies and groups, among which 67 925 contain at least two Friends-of-Friends (FoF) members and 44 441 are galaxy pairs. (Here, we just simply refer the groups with two members as the pairs.) Throughout this paper, we refer to the brightest galaxies as the central galaxies of the groups, and all other member galaxies as satellites.

As one of the fourth generation of SDSS (SDSS-IV; Blanton et al. 2017), MaNGA (Bundy et al. 2015) has accomplished its task on mapping the kinematic structure and detailed composition of more than 10 000 nearby galaxies with stellar mass $\log M_*/{\rm M}_\odot > 9.0$ and redshifts range of $0.001 < z < 0.15$. MaNGA has obtained spatially resolved spectra within the central 1.5–2.5 effective radii of galaxies with 1–2 kpc physical sampling (Drory et al. 2015), thanks to its 17 IFUs. It provides a wavelength coverage of 360–1000 nm and a spectral resolution of $R \sim 2000$ (Bundy et al. 2015). These spectra provide us with two-dimensional maps of stellar kinematics, star formation rate, stellar metallicity, and so on. The observed ∼10 000 galaxies spread across ∼2700 deg^2 of the sky. No special selection criteria on apparent size or inclination are made, so these galaxies are representative samples in the local Universe. In this paper, we used the stellar kinematic maps from the newest Data Analysis Pipeline (DAP; Belfiore et al. 2019; Westfall et al. 2019) output in Data Release 17 (DR17; Abdurro'uf et al. 2022) and the corresponding summary table called the DAPall catalogue. The $DAPTYPE$ (see MaNGA analysis pipeline website) of the kinematic maps we used was labelled as $VOR10-MILESHC-MASTARSSP$, meaning that the map spaxels are binned to S/N ∼ 10 using the Voronoi binning algorithm (Cappellari & Copin 2003), that the stellar kinematics are determined using the $MILESHC$ template library (Westfall et al. 2019), and that the stellar continuum are fitted by the $MASTARSSP$ templates (Abdurro'uf et al. 2022). After matching the MaNGA galaxies with YangDR7, we obtain 2429 central galaxies that have at least one satellite member. Among them, 2428 centrals are labelled with morphological types obtained from the MaNGA Deep Learning DR17 Morphology catalogue (Domínguez Sánchez et al. 2022) and the distribution of galaxy types is shown in upper panel of Fig. 1. To avoid edge effect, which accounts for the fact that a group may partly fall out of the survey edges, but not to reduce our sample size too much, we give a cut to let the edge factor larger than 0.9 (edge factor of 1 means no edge effect), leaving 688 LTGs and 133 S0s.

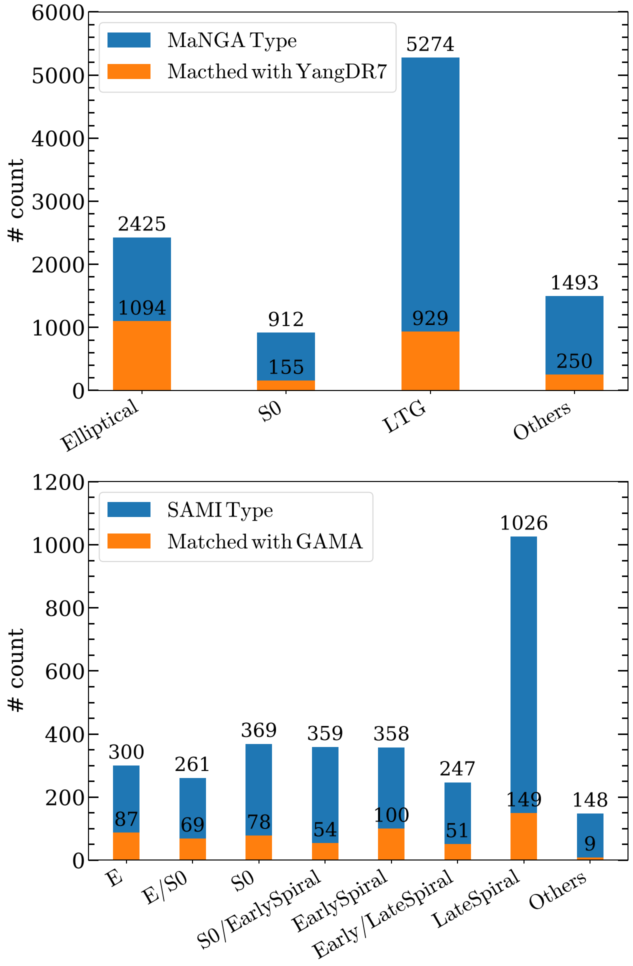

Figure 1. The statistics of galaxy types of MaNGA (upper panel) and SAMI (lower panel) for all galaxies (blue) and matched centrals (orange). The x-axis shows the different galaxy morphology types defined in each survey and the numbers on the histograms are the corresponding counts.

2.2 The GAMA and SAMI

The heart of the GAMA (Driver et al. 2011) project is a spectroscopic survey aiming at measuring ∼300 000 galaxies in detail using the AAOmega multi-object spectrograph on the Anglo-Australian Telescope (AAT). The project is divided into three distinct phases, GAMA I (Baldry et al. 2010), GAMA II (Liske et al. 2015; Baldry et al. 2018), and GAMA III (GKV; Bellstedt et al. 2020; Driver et al. 2022). Until now, the GAMA team has released the fourth and final GAMA data release (DR4; Driver et al. 2022), which will be updated when new versions of data are available. In this paper, we used the catalogues of GAMA II in GAMA DR4 for our analysis. The GAMA II catalogues cover three different survey regions: equatorial, G02, and G23 (see GAMA webpage[1] for details), containing ∼460 000 science targets. The GAMA data is arranged as the so-called Data Management Units (DMUs), each of which contains a particular type of catalogue data or tables. The GROUPFINDING DMU (Robotham et al. 2011) provides group catalogues for GAMA galaxies in equatorial and G02 regions, giving 26 194 groups with at least two FoF members out of 83 093 galaxies.

The SAMI (Croom et al. 2012) is a new instrument on the 4-m AAT equipped with integral field spectroscopy instrument, which allows us to spatially measure galaxies in great detail. Recently, the newest SAMI Data Release 3 (DR3; Croom et al. 2021) containing 3068 galaxies and their value-added data products (such as visual morphology) have been available. These galaxies have stellar masses ranging from 10^8 to 10^{12} $\mathrm{M}_\odot$ with redshift range of $0.004 < z < 0.115$. The SAMI instrument has 13 so-called hexabundles, each of which contains 61 optical fibres with each subtending 1.6 arcsec, giving a total diameter of 15 arcsec for one bundle (Bryant et al. 2014). The angular resolution of SAMI is expected to be ∼2.1 arcsec considering seeing. For spectral sampling, SAMI has a resolution of $R \sim 1700$ in the blue arm with a wavelength coverage of 3700–5700 Å and a resolution of $R \sim 4500$ in the red arm covering a wavelength range of 6300–7400 Å (Bryant et al. 2015). The stellar kinematics in SAMI are derived using penalized Pixel-Fitting code (PPXF; Cappellari & Emsellem 2004; Cappellari 2017). Matching SAMI galaxies with the GAMA group catalogue we obtained 597 groups, where 432 centrals are spirals/S0s. The morphologies of all SAMI galaxies are visually classified (see Cortese et al. 2016 for details) by the team through SDSS or VST/ATLAS RGB composite images and are available in VISUALMORPHOLOGYDR3 catalogue. The counts of different types are shown in the lower panel of Fig. 1. Among all of the centrals, 562 galaxies have well-defined kinetic position angles (PAs). Criterion that `GroupEdge` value of groups shall be larger than 0.9 is also applied, leaving 400 spirals/S0s.

3 METHODOLOGY

3.1 Stacking the kinetic fields of host stellar discs and satellites

In fig. 9 of Lu et al. (2022), the authors demonstrated the co-rotation signals by stacking the line-of-sight (LOS) velocity maps of the ambient cold CGM gas and satellites of TNG-100 galaxies according to their corresponding stellar discs. The steps therein are summarized as follows: first all galaxy discs were rotated to their edge-on configurations using the corresponding rotational matrices; secondly a random disc inclination between -60° and 60° was applied to each simulated galaxy around the major axis considering that observed galaxies are rarely perfectly edge-on. The redshifted sides of galaxy discs were all put on the same side in the sky plane during stacking. Finally, the same operations were done for all satellite galaxies and the CGM gas cells. After stacking, a coherent pattern in the LOS kinematics appears among the galaxy discs, the associated cold CGM gas, and the satellite galaxies in the environment.

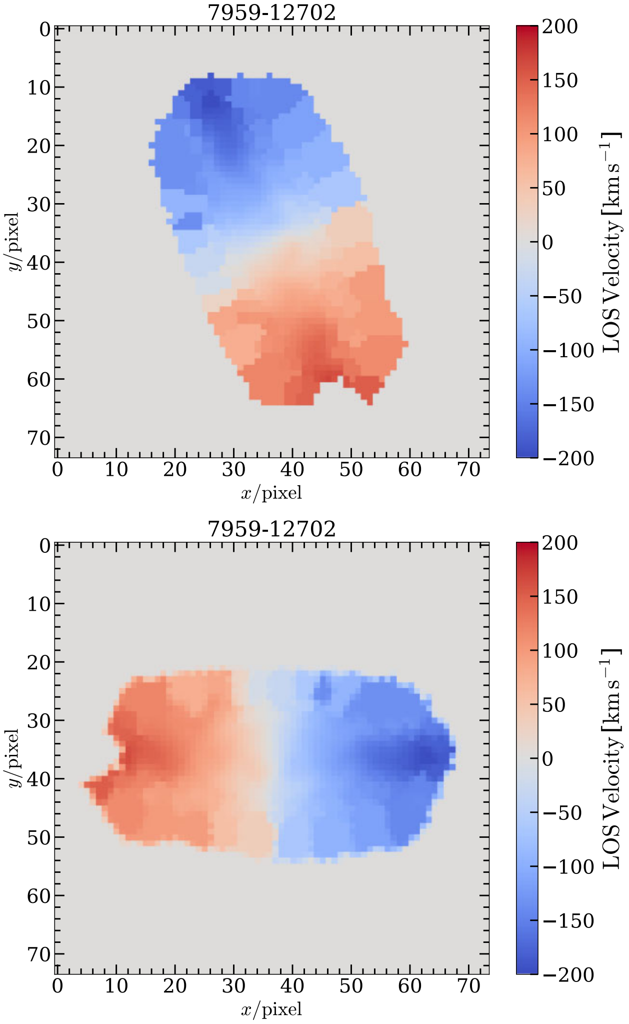

Figure 2. An example (from MaNGA, Plate-IFU: 7959−12702) on the rotation of the stellar discs. We rotate the original kinematic map (top panel) such that the kinetic major axis of the disc is then along the *x*-axis (bottom panel). We always make sure that the redshifted (blueshifted) part lies on the left (right) side of the *x*-axis. The colour shows the LOS velocities of pixels.

When dealing with the collected observational data in this work, we took a similar approach but with a few differences due to the limitation of the data. Both MaNGA and SAMI provide catalogues of morphological type of galaxies, based on which we first selected late-type galaxies (LTGs) and S0 galaxies for MaNGA and all spirals and S0 galaxies for SAMI as our stacking samples because of their well-recognized stellar discs. As we have no idea about the rotation matrices of galaxies in their sightlines, so we selected galaxies that appear nearly edge-on with clear rotation kinematic (see Fig. 2). We note that although MaNGA also gives a parameter in its morphological catalogue describing whether the galaxy is edge-on, the edge-on criterion is too strict to result in any sizable statistical sample (113 LTGs/25 S0s in 688 LTGs/133 S0s). We therefore did

---

[1] http://www.gama-survey.org/dr4/.

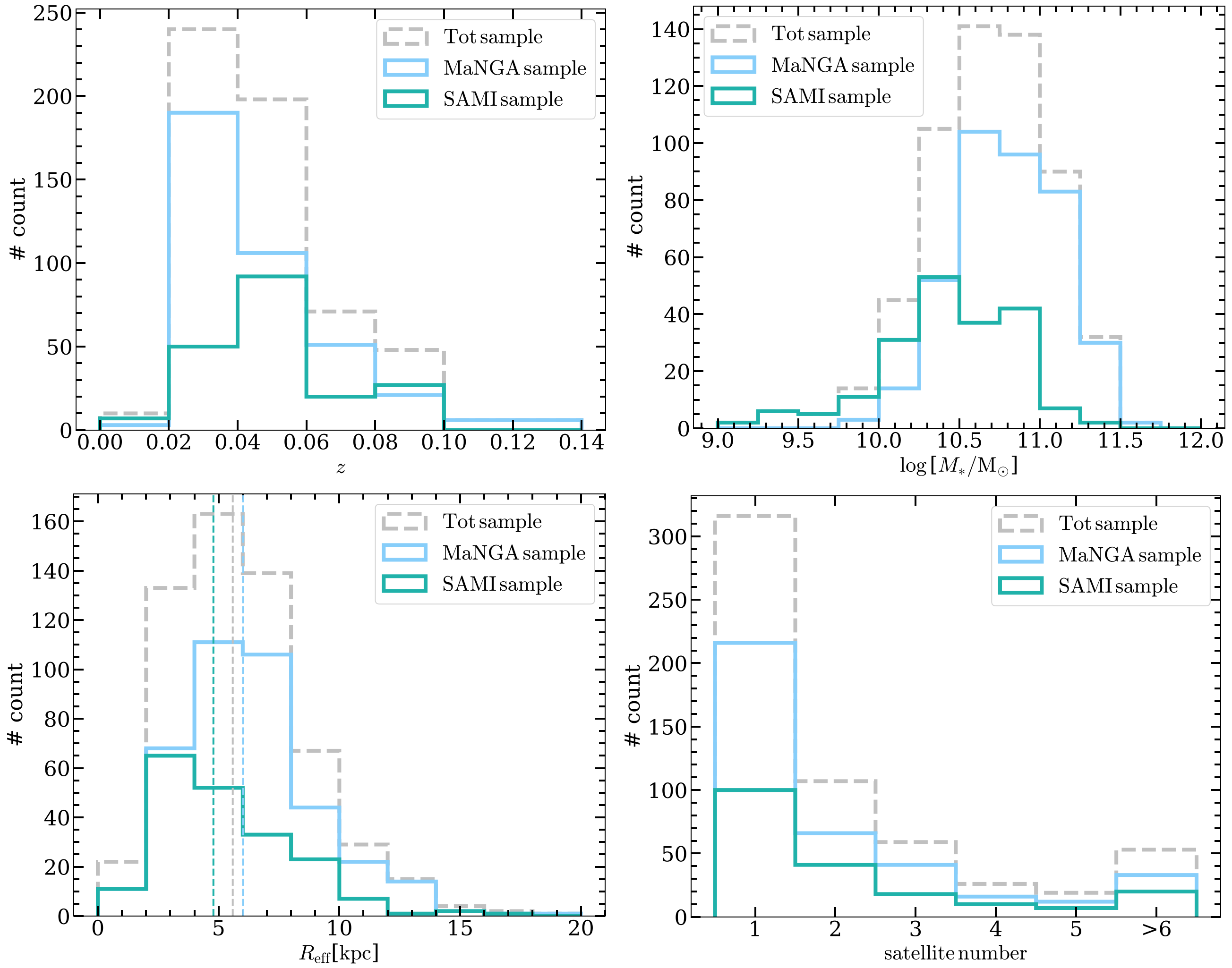

Figure 3. The distribution of central redshift, central stellar mass, central effective radius, and the satellite number of the selected samples. Silver, blue, and green lines are for tot samples, MaNGA samples, and SAMI samples, respectively. Vertical lines in the lower left panel represent the medians.

NOT adopt the MaNGA edge-on parameter as indication. Instead, we took a visual inspection approach through images and two-dimensional velocity maps, and finally obtained 326 LTGs and 58 S0s for MaNGA galaxies, and 196 spirals/S0s for SAMI galaxies that have kinematic maps with good sense of rotations. The statistics (i.e. redshift, stellar mass, effective radius, and satellite numbers) of the selected systems are shown in Fig. 3. The stellar masses of the selected galaxy samples span a range of $\log M_*/\mathrm{M}_\odot \in [9.0,\ 11.5]$. The median effective radii of the two galaxy sample are about 5 kpc. Most of the systems have one or two satellites.

We then took the kinematic PA of each central galaxy to rotate the overall kinematic field. The adopted PAs for MaNGA galaxies were derived from Zhu et al. (2023), which adopted the PAFIT[2] package and the PAs for SAMI galaxies were calculated using the FIT_KINEMATIC_PA code. Both of them are derived using the algorithm described in appendix C of Krajnović et al. (2006).

The kinematic PA of each central galaxy was then used to rotate the stellar kinematic map, as well as the associated satellites galaxies such that the projected major axis is along the x-axis as is presented in Fig. 2. A further rotation was given to make the redshifted (blueshifted) side of the stellar kinematic map appear on the left-hand (right-hand) side during stacking.

As the galaxy sample spans a stellar mass range over two orders of magnitudes, a further normalization on the projected separation is required before stacking in order to eliminate the mass dependence. To do so, we scaled the physical distances along the projected major axis with the corresponding effective radius $R_{\rm eff}$, and those along the minor axis by $\frac{b}{a}R_{\rm eff}$, where $\frac{b}{a}$ is the projected axial ratio of the central galaxy.

3.2 Distinguishing the red- and blueshifted satellites

Considering the spectral resolution and the fact that satellites with too high relative velocities are not likely to be bound to the systems, we further retained satellites with relative LOS velocities (see below for details) ranging from 30 to 500 km s^{-1}. The LOS velocities of satellites relative to their centrals are calculated based on the assumptions that the centrals present no peculiar motions and the peculiar motions of satellites are non-relativistic. The relative LOS

---

[2] Version 2.0.7, from https://pypi.org/project/pafit/.

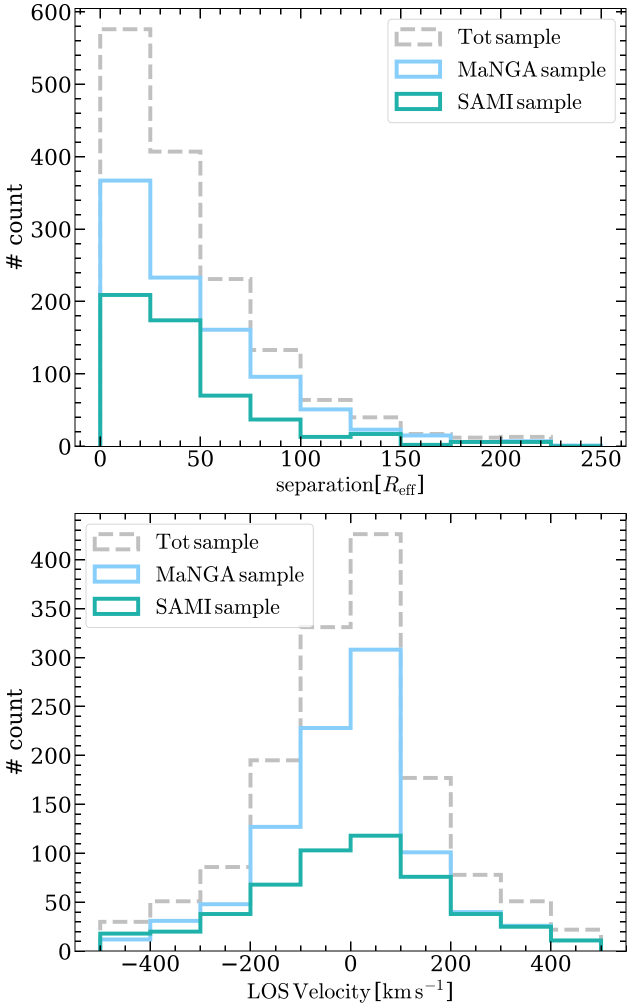

Figure 4. Histograms of the satellite projected separations (top) and LOS velocities (bottom) relative to the central galaxies.

velocity is defined as

$$\Delta v_{\rm los} = \frac{z_{\rm s} - z_{\rm c}}{1 + z_{\rm c}}\, c, \quad (1)$$

where $z_{\rm c}$ and $z_{\rm s}$ are the redshifts of the central and satellite galaxies, respectively; c is the speed of light. The statistics of the satellite projected separations and LOS velocities are presented in Fig. 4

If satellite galaxies indeed exhibit coherent kinematics as the central stellar discs, one would expect that the redshifted (blueshifted) satellites shall be preferentially distributed on the redshifted (blueshifted) side of the stellar discs of the host galaxies and therefore the stacked (normalized) separation distribution along the major axis of the redshifted satellite galaxies shall be significantly different from that of the blueshifted satellite population. To quantitatively describe this difference, we applied Kolmogorov–Smirnov (K–S) test to the two distributions using the PYTHON package named NUMPY,[3] which provides us a p-value, indicating the probability that the two distributions come from the same underlying distribution. The lower p is, the larger the difference is between the two distributions.

We also ran random tests to our samples. We maintained the radial ordering of the stacked distribution but assigned a random angle relative to the major axis to each satellite, resulting in one particular realization of random angular distribution. Then we did K–S test, giving us a p-value. After repeating this sampling and testing process for enough times (e.g. 100 000 times), we obtained a group of distributions and p-values. The 1σ regions of these distributions along major axis and the median with the standard deviation of the p-values are taken as the result of the random tests.

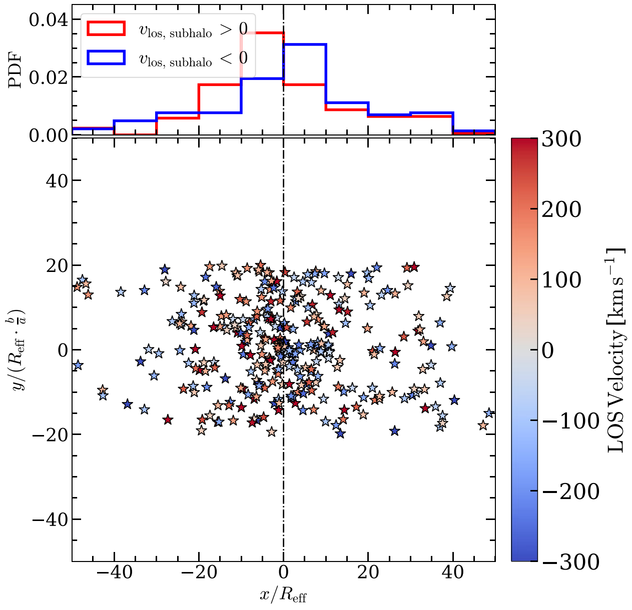

Figure 5. The stacked distribution of satellites colour-coded by the LOS velocities relative to their corresponding central galaxies. All central galaxies are rotated according to their kinetic PAs such that the kinetic major axes are all along the x-axis; and the redshifted and blueshifted side are put to the left- and right-hand side of the figure, respectively. The x-axis and y-axis are the normalized projected physical scale calculated at the central's redshift with the corresponding cosmology (see Section 1). The star symbols represent the collections of the satellites, which are rotated accordingly and that meet the criteria of $|y| < 20\, R_{\rm eff}\cdot\frac{b}{a}$. The histograms on the top of the panel show the distribution of these satellites along the major axis, with the red and blue lines for the positive and negative LOS velocities, respectively. Black dash–dotted line marks the $x = 0$.

The other way to test the coherent kinematics is that if the coherent signal exists, the satellites that satisfy $x < 0$ (i.e. on the redshifted side of the stellar discs) would preferentially exhibit redshifted LOS velocities; those with $x > 0$ would prefer blueshifted LOS velocities. We quantified the difference between the two LOS velocity distributions also using the K–S test. Again, a smaller value of p indicates a lower chance of the two distributions are intrinsically the same.

4 RESULTS

According to the structure formation and evolution theory, there should be expected correlations between large and small scales as have been seen in various simulations (e.g. Aragón-Calvo et al. 2007; Hahn et al. 2007; Libeskind et al. 2013a, b; Wang et al. 2018; López et al. 2021) and observations (e.g. Lee & Erdogdu 2007; Lee et al. 2019a, b; Kraljic et al. 2021; Barsanti et al. 2022; Tudorache et al. 2022). Here, we study the coherent dynamics between the central discs and their satellites by stacking all samples, as is shown in Fig. 5. From this relative spatial configuration, we see that the redshifted (blueshifted) satellites are preferentially distributed on the redshifted

---

[3] https://numpy.org.

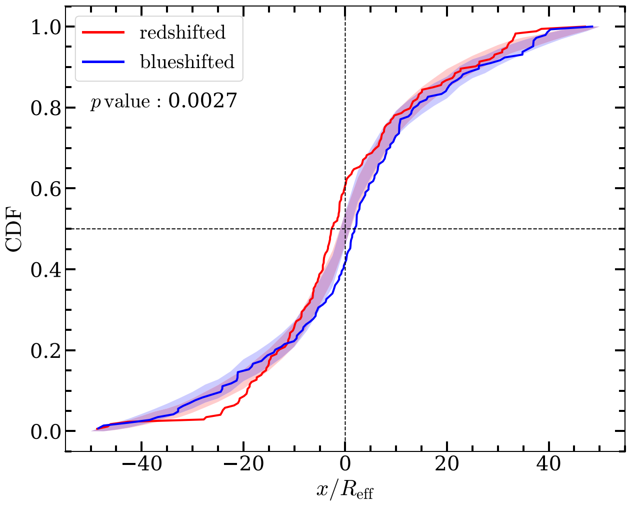

Figure 6. The CDFs along the major axis of the satellites in Fig. 5 for all redshifted and blueshifted members (red and blue lines) but restricted to the same region. Solid lines are the distributions for real data, while shaded parts are the 1σ regions of the 100 000 random angular sampling tests. Dashed vertical and horizontal lines represent the zero-point along the major axis and CDF value of 0.5. On the upper left shows the p-value of the K–S test between blueshifted and redshifted species.

(blueshifted) side of the stellar discs of the host galaxies, and a significant difference appears between the distributions of satellites along the major axis (i.e. red and blue histograms), especially at scales within $\pm 20\,R_{\rm eff}$, about ±100 kpc. This difference indicates a preferential coherent rotation between satellite galaxies and the stellar discs of host galaxies and the scale is totally comparable with the simulated results from the TNG-100 simulation, as is shown in fig. 9 of Lu et al. (2022).

In order to quantify the differences between these two distributions, we applied a Kolmogorov–Smirnov test and the result is displayed in Fig. 6. The blue and red solid lines are the cumulative distribution functions (CDFs) of the projected separation along the major axis for the blueshifted and redshifted satellite galaxies, respectively. The dashed vertical and horizontal lines show the zero-point on the x-axis and the 50 per cent accumulation points of the CDF. The CDF value of blueshifted satellites (blue solid line) is about 0.43 at $x = 0$, indicating an asymmetric distribution towards the blueshifted part of the stellar discs. The same but more asymmetric signal is seen for the redshifted satellites, for which the CDF at $x = 0$ is ∼0.62. Through a K–S test, we found a p-value of ∼0.0027, indicating that the hypothesis that the two distributions are the same can be ruled out at $\sim 3\sigma$ level, or in other words, that the redshifted and blueshifted data are totally different distributions at a confidence level of at least 99.7 per cent. The fact that the redshifted (blueshifted) satellites preferentially projected on the $x < 0$ ($x > 0$) side, implies the expected coherent rotation between satellites and the central discs. The 1σ regions (shaded) of the random tests show nearly no preferential distributions and the median of the p-values ($\sim 0.56^{+0.31}_{-0.36}$) indicates that this kinematical coherence can hardly be drawn from the random distributions.

In addition to splitting the population to the redshifted and blueshifted parts by their LOS velocities and examining the difference in their offset preferences, we also divided the satellites into two groups with $x > 0$ and $x < 0$ and compared their LOS velocity distributions. The result is shown in Fig. 7. According to our stacking procedures in Section 3.1, $x > 0$ and $x < 0$ actually correspond to the blueshifted and redshifted parts of the stellar discs. The K–S test shown in Fig. 8 indicates the two distributions are different at a confidence level of 99.96 per cent ($\sim 3.5\sigma$, with p-value of 0.0004). The fact that the satellites with $x > 0$ ($x < 0$) exhibit an LOS velocity distribution towards the blueshifted (redshifted) case, same as that of the stellar disc rotation direction, again implies the co-rotation between the stellar discs and satellites.

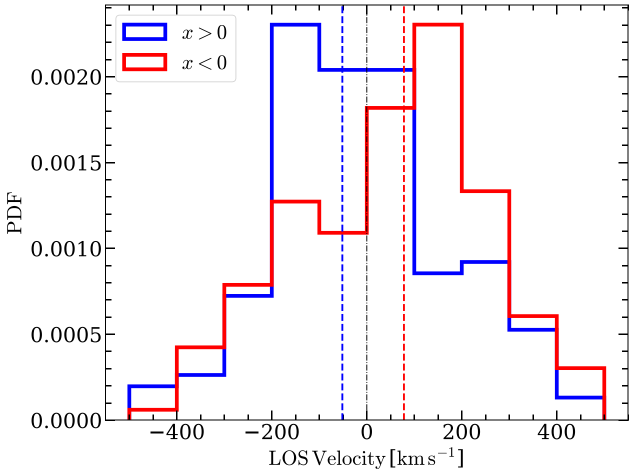

Figure 7. LOS velocity distributions of the satellites shown in Fig. 5. Blue and red solid lines are the histograms for satellites with $x > 0$ and $x < 0$, respectively, while dashed lines are the corresponding medians of the distributions. The black dash–dotted line just indicates the LOS velocity of zero.

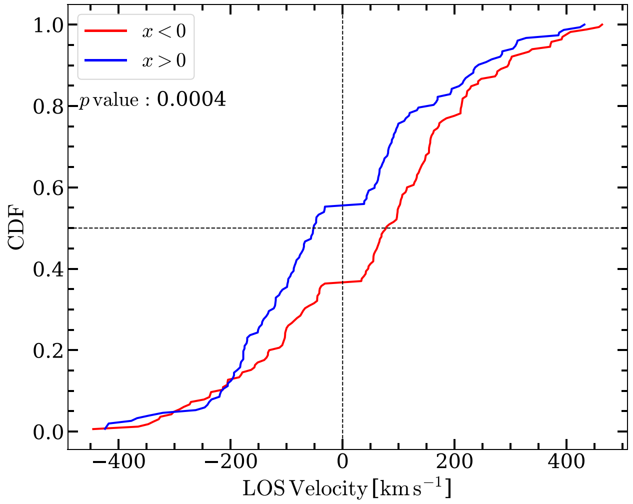

Figure 8. The CDFs of the distributions in Fig. 7. Red and blue lines are for the $x < 0$ and $x > 0$ species. Dashed vertical and horizontal lines represent the LOS velocity of zero and CDF value of 0.5. Upper left is the p-value of the K–S test between these two distributions. The platforms of the two distributions near the zero-point are due to the cut of LOS velocities larger than 30 $\rm km\,s^{-1}$.

5 CONCLUSIONS AND DISCUSSIONS

In this paper, using two sets of observation data, i.e. the SDSS and MaNGA galaxy survey, and the GAMA and SAMI galaxy survey, we carry out a search for a coherent kinematic signal between the stellar discs and their ambient galaxies, as predicted in the TNG-100 simulation and explicitly demonstrated by Lu et al. (2022).

To do so, we selected the late-type and S0 central galaxies that show clear patterns of regular stellar-disc rotation through visual inspection in the MaNGA and SAMI galaxy surveys, rotated and stacked the kinematic field of these systems (see Section 3.1) to search for the predicted coherent kinematics. A K–S test showed that the distributions of the projected locations of the redshifted and the blueshifted satellite populations differ at a confidence level of 99.7 per cent ($\sim 3\sigma$, see Section 4 and Figs 5 and 6 therein). In particular, the difference is as such that the redshifted (blueshifted) satellites are preferentially distributed on the redshifted (blueshifted) side of the stellar discs of the host galaxies. We also ran random tests to our samples (see Fig. 6), which shows the co-rotation can hardly be derived from random distribution. While the two populations that are divided according to their projected locations with respect to the central stellar disc also exhibit different LOS velocity distributions. The confidence level for such a difference is 99.96 per cent ($\sim 3.5\sigma$, see Figs 7 and 8). The difference is present as such that satellite galaxies projected on the redshifted (blueshifted) of the rotating stellar discs also preferentially have redshifted (blueshifted) LOS velocities. All tests above confirm the prediction that the satellites are co-rotating with the central stellar discs.

The co-rotation signal, as is presented in Fig. 5, is significant at about 100 kpc ($\sim \pm 20\, R_{\mathrm{eff}}$) and becomes weaker when going to larger scales. According to the angular momentum acquisition and modulation scenario (Lu et al. 2022; Wang et al. 2022), the spin of the stellar disc is an inheritance of the cold CGM, the spin of which is further modulated by its ambient environment (satellites) through interactions like merging and fly-by. It is worth noting that the coherent kinematic signal is exactly the consequence of such an angular momentum inheritance from large to small scales. However, this can only be observed when stacking a sizeable sample of galaxies in their merging and interacting environment. On individual cases, the cold CGM gas is always in form of localized in-spiral streams (see figs 4 and 8 of Wang et al. 2022) rather than a butterfly-like accretion disc, which can only be seen after stacking (see fig. 9 of Lu et al. 2022). Equally, the multidirection galaxy accretion would not guarantee that we observe coherent rotations of satellites around each and every individual host. The coherent kinetic signal as reported in this work can only be seen after stacking systems lined up according to kinematic major axes of the stellar discs.

Our discovery is generally consistent with previous observational studies on the co-rotation between galaxies (i.e. their stellar discs) and their environment. In Lee et al. (2019a), the author found clear evidence (3.5σ) of dynamical coherence (measured by luminosity-weighted velocity difference in neighbouring galaxies that are projected on different kinematic sides of central galaxies) existing between galaxy *outskirts* and their neighbours (*not only satellites*), up to 800 kpc using the CALIFA (Sánchez et al. 2012) survey data and NASA-Sloan Atlas (created by Michael Blanton) catalogue. The coherent signal gets stronger at smaller distances within 300 kpc (see fig. 11 therein). Lee, Pak & Lee (2020) further showed that the small-scale dynamical coherence is also accompanied by galaxy conformity, indicating that galaxy interactions are responsible for both observations. In Lee et al. (2019b), the authors claimed that such a dynamical coherence can extend up to ~6 Mpc (at 2.8σ), which is still not well explained. It is interesting to note that Mai et al. (2022), following a similar method as Lee et al. (2019b), however, did not detect similar coherent signals as up to a projected distance of 10 Mpc from central galaxies. They also suggested that the coherence at larger scales might be caused by the coincidental scatter or the variance of LSS rather than physical relations between galaxy spins and their neighbours.

In general, galaxy systems are born in their large-scale environment. Their evolution is also largely shaped by the large-scale field. The large-scale matter distributions of cosmic structures set up initial conditions for galaxies to be born with and also determine how materials like gas and gravitationally bound haloes at smaller scales are accreted from nearby cosmic webs to galaxy centres. The former flows into a galaxy's centre and forms stars, while the latter become satellites (or passers-by) and provide modulations to the galaxy through interactions. Here in this paper, we search for a co-rotation pattern among galaxy groups, which is only significant at scales of 100 kpc. It would be interesting to investigate how far this signal may extend to, as a consequence of co-evolution of galaxies in their large-scale environment.

ACKNOWLEDGEMENTS

We would like to thank Prof. Xiaohu Yang for his patience when we had troubles with the catalogue data. We are also grateful to Yanhan Guo for his kind help on the explanation and data of volume corrections. Also, we want to thank Prof. Simon White for his constructive suggestions about the statistics on the kinematical coherence.

DATA AVAILABILITY

YangDR7 catalogues are available from https://gax.sjtu.edu.cn/data/Group.html. The other group and galaxy data are obtained from official websites of MaNGA, GAMA, and SAMI survey. The rest of the data used in the article will be shared on reasonable request.

REFERENCES

Abazajian K. N. et al., 2009, ApJS, 182, 543
Abdurro'uf et al., 2022, ApJS, 259, 35
An S.-H., Kim J., Moon J.-S., Yoon S.-J., 2021, ApJ, 914, 86
Aragón-Calvo M. A., van de Weygaert R., Jones B. J. T., van der Hulst J. M., 2007, ApJ, 655, L5
Baldry I. K. et al., 2010, MNRAS, 404, 86
Baldry I. K. et al., 2018, MNRAS, 474, 3875
Barsanti S. et al., 2022, MNRAS, 516, 3569
Belfiore F. et al., 2019, AJ, 158, 160
Bellstedt S. et al., 2020, MNRAS, 496, 3235
Blanton M. R. et al., 2005, AJ, 129, 2562
Blanton M. R. et al., 2017, AJ, 154, 28
Bryant J. J., Bland-Hawthorn J., Fogarty L. M. R., Lawrence J. S., Croom S. M., 2014, MNRAS, 438, 869
Bryant J. J. et al., 2015, MNRAS, 447, 2857
Bundy K. et al., 2015, ApJ, 798, 7
Cappellari M., 2017, MNRAS, 466, 798
Cappellari M., Copin Y., 2003, MNRAS, 342, 345
Cappellari M., Emsellem E., 2004, PASP, 116, 138
Cortese L. et al., 2016, MNRAS, 463, 170
Croom S. M. et al., 2012, MNRAS, 421, 872
Croom S. M. et al., 2021, MNRAS, 505, 991
Domínguez Sánchez H., Margalef B., Bernardi M., Huertas-Company M., 2022, MNRAS, 509, 4024
Doroshkevich A. G., 1970, Astrofizika, 6, 581
Driver S. P. et al., 2011, MNRAS, 413, 971
Driver S. P. et al., 2022, MNRAS, 513, 439
Drory N. et al., 2015, AJ, 149, 77
Firmani C., Avila-Reese V., 2000, MNRAS, 315, 457
Firmani C., Avila-Reese V., 2009, MNRAS, 396, 1675

Hahn O., Porciani C., Carollo C. M., Dekel A., 2007, MNRAS, 375, 489

Kim Y., Smith R., Shin J., 2022, ApJ, 935, 71

Krajnović D., Cappellari M., de Zeeuw P. T., Copin Y., 2006, MNRAS, 366, 787

Kraljic K., Duckworth C., Tojeiro R., Alam S., Bizyaev D., Weijmans A.-M., Boardman N. F., Lane R. R., 2021, MNRAS, 504, 4626

Lee J., Erdogdu P., 2007, ApJ, 671, 1248

Lee J. H., Pak M., Lee H.-R., Song H., 2019a, ApJ, 872, 78

Lee J. H., Pak M., Song H., Lee H.-R., Kim S., Jeong H., 2019b, ApJ, 884, 104

Lee J. H., Pak M., Lee H.-R., 2020, ApJ, 893, 154

Libeskind N. I., Hoffman Y., Forero-Romero J., Gottlöber S., Knebe A., Steinmetz M., Klypin A., 2013a, MNRAS, 428, 2489

Libeskind N. I., Hoffman Y., Steinmetz M., Gottlöber S., Knebe A., Hess S., 2013b, ApJ, 766, L15

Liske J. et al., 2015, MNRAS, 452, 2087

López P., Cautun M., Paz D., Merchán M., van de Weygaert R., 2021, MNRAS, 502, 5528

Lu S. et al., 2022, MNRAS, 509, 2707

Mai Y. et al., 2022, MNRAS, 515, 984

Marinacci F. et al., 2018, MNRAS, 480, 5113

Mo H. J., Mao S., White S. D. M., 1998, MNRAS, 295, 319

Moon J.-S., An S.-H., Yoon S.-J., 2021, ApJ, 909, 34

Naiman J. P. et al., 2018, MNRAS, 477, 1206

Nelson D. et al., 2018, MNRAS, 475, 624

Nelson D. et al., 2019, MNRAS, 490, 3234

Peebles P. J. E., 1969, ApJ, 155, 393

Pillepich A. et al., 2018, MNRAS, 475, 648

Pillepich A. et al., 2019, MNRAS, 490, 3196

Robotham A. S. G. et al., 2011, MNRAS, 416, 2640

Sánchez S. F. et al., 2012, A&A, 538, A8

Springel V. et al., 2018, MNRAS, 475, 676

Tudorache M. N. et al., 2022, MNRAS, 513, 2168

Wang P., Guo Q., Kang X., Libeskind N. I., 2018, ApJ, 866, 138

Wang S., Xu D., Lu S., Cai Z., Xiang M., Mao S., Springel V., Hernquist L., 2022, MNRAS, 509, 3148

Westfall K. B. et al., 2019, AJ, 158, 231

White S. D. M., 1984, ApJ, 286, 38

White S. D. M., Frenk C. S., 1991, ApJ, 379, 52

White S. D. M., Rees M. J., 1978, MNRAS, 183, 341

Yang X., Mo H. J., van den Bosch F. C., Pasquali A., Li C., Barden M., 2007, ApJ, 671, 153 (YangDR7)

York D. G. et al., 2000, AJ, 120, 1579

Zhu K., Lu S., Cappellari M., Li R., Mao S., Gao L., 2023, MNRAS, 522, 6326

This paper has been typeset from a TEX/LATEX file prepared by the author.